

PLASMA TERMINATION BY EXCESS PELLET FUELING AND IMPURITIES IN TJ-II, LHD AND WENDELSTEIN 7-X

A.Dinklage^{1,2*}, K.J. McCarthy³, C. Suzuki⁴, N. Tamura⁴, Th. Wegner¹, H. Yamada^{4,5}, J. Baldzuhn¹, B. Buttenschön¹, H. Damm¹, P. Drewelow¹, G. Fuchert¹, H. Kasahara⁴, D. Maier⁶, J. Miyazawa⁴, G. Motojima⁴, T. Oishi⁴, T. Sunn Pedersen^{1,2}, R. Sakamoto⁴, R.C. Wolf^{1,7}, D. Zhang¹, the W7-X Team, the LHD Experiment Group and the TJ-II Team

¹Max-Planck-Institut für Plasmaphysik
Greifswald, Germany

*Email: dinklage@ipp.mpg.de

²E.-M.-Arndt Universität Greifswald, Greifswald, Germany

³CIEMAT, Madrid, Spain

⁴National Institute for Fusion Science, National Institutes of Natural Sciences, Toki, Japan

⁵Tokyo University, Tokyo, Japan

⁶Universität Greifswald, Greifswald, Germany

⁷Technische Universität Berlin, Berlin, Germany

Abstract

Plasma terminating events due to excess pellet fueling and impurity injection is studied in LHD, W7-X and TJ-II. Time scales for these events range from values of a decimal fraction of typical energy confinement times to the order of the energy confinement time. The leading mechanism of energy loss appears to be radiation revealing similarities to radiation collapses when a radiative density limit is approached. Differently to tokamaks, the capability of helical devices to provide magnetic confinement in vacuum (i.e. without large inductive plasma currents) gives rise to the observation of plasma recovery even after some energy confinement times. Time-scales and the dynamics of recovery for close to marginal termination indicates some robustness in the response of helical devices to large unintended perturbations.

1. INTRODUCTION

It appears to be self-evident that the unintended termination of plasma operation could lead to safety relevant interruptions in potential fusion reactors. Potential causes may be due to plasma stability or sorts of ‘external events’, e.g. the release of material from plasma facing components due to mechanical fatigue. Sudden termination of plasma operation accompanied by a release of particles and energy is an aspect that enters material requirements in terms of power loads, localization, forces (e.g. by fast breakdown of plasma currents). In tokamaks, such events may lead to disruptions or thermal quenches. As one of the main findings in this paper, stellarators appear to have the potential for the recovery of plasmas close to marginal termination. While unintended plasma termination is unpredictable in general, operating present experiments may deliver the basis for validated models predicting the impact of plasma termination. These models may serve for defining safety margins and the reliability of which appears to be important input for licensing procedures. The identification of potential recovery (and thereby the exclusion of *false positives*) after an unexpected event in a stellarator may also serve for more robust control schemes in reactor scale experiments.

A broader study of plasma termination, however, is lacking for helical devices and this paper is intended to provide an initial overview of unintended plasma termination in the large helical device (LHD), Wendelstein 7-X (W7-X) and TJ-II. Radiative collapses frequently observed in discharges with highly-radiating edge and scrape-off layer (SOL) regions, however, are not covered in this study but will be reported elsewhere in the context of radiative density limits [1] early addressed in helical devices by experimental [2] and theoretical [3] studies. While disruptions are not expected in (currentless) stellarator/heliotron operation, thermal quenches are certainly to be illuminated for reactor scale stellarators and heliotrons as well. Being not a subject of this study, but relevant to the introduced motivation, very recently, observations on W7-X showed fast loss of plasma energy when large

and broadly distributed (in excess to expected boot-strap currents) current drive was applied on plasmas in W7-X.

As an initial systematic study on plasma termination in large stellarators and heliotrons, benefit is taken from the fact that both W7-X and the LHD, are sufficiently large to address key questions for potential helical fusion reactors since their size allows to study plasmas at low collisionality. Both devices are equipped with superconducting coils to achieve true long-pulse operation. Complementary aspects are delivered from experiments in TJ-II. The methods employed in this study rely on the analysis of waveforms of temporally varying data and the spatio-temporal evolution after large amounts of fuelling pellets or impurities are injected into the helical plasma. This approach allows the quantification of perturbative material and variations reveal the level of injected matter allowing the recovery to stable plasma operation. This study will provide a documentation of selected cases of plasma termination in different devices and a comparison of typical time scales. The paper gives further introduction of the devices compared in this study and discusses plasma termination due to excess fuelling and excess impurity injection by tracer-encapsulated impurity pellets (TESPEL) or laser blow-off (LBO).

2. SURVEY OF DEVICES

Employing different helical confinement concepts in comparative studies takes benefit from a larger configuration space and potential effects of plasma volume or the structure of the magnetic field [4]. The devices include in this study vary in both aspects.

The large helical device (LHD) [5] is a heliotron equipped with super-conducting coils starting operation in 1998 in Toki (Japan). The nominal major plasma radius is $R = 3.75$ m, the minor radius $a = 0.6$ m (both varying when the magnetic field structure is changed at typical fields up to 2.9T). LHD is equipped with 23 MW of heating power from neutral beam injection, 2.5 MW from ECRH and 3MW of ICRH. LHD plasmas show electron temperature up to 4keV and electron densities up to $1.2 \times 10^{21} \text{m}^{-3}$ (the latter in the super-dense core regime but at low temperatures) and bulk ion temperatures of up to 10keV. It is noted that specific values of all aforementioned parameters are subject to the discharge scenario (as for the W7-X and TJ-II below). LHD is equipped with a pellet injector delivering fuelling pellets [6] and tracer encapsulated solid pellets (TESPEL) [7]. Excess injection of both was observed to terminate the plasma operation (cf. Sec. 3.1 and 3.2).

Wendelstein 7-X (W7-X) is a superconducting HELIAS (helical axis advanced stellarator) with a major radius of $R = 5.5$ m and typical minor radius of $a = 0.5$ m. W7-X started operation in 2015 in Greifswald (Germany) [8] and is equipped with about 7 MW electron cyclotron resonance heating (ECRH). W7-X is equipped with a pellet injection system [9] and a laser blow-off diagnostics [10].

TJ-II is a heliac operated since 1997 in Madrid (Spain) [11]. The device has a major radius of $R = 1.5$ m and an average minor radius of $a < 0.22$ m. It is equipped with ECRH and neutral beam injection heating (NBI). With ECRH the plasma density cut-off is $1.7 \times 10^{19} \text{m}^{-3}$. A fuelling pellet injection system was commissioned in 2014 [12]. More recently the pellet injector was temporally equipped with a TESPEL tracer-loaded pellet system [13].

3. EXPERIMENTAL FINDINGS

3.1. Fuelling pellet injection on LHD

LHD is equipped with a 20 barrel solid hydrogen injector [14] delivering high fuelling rates even adjustable to terminate the plasmas. An example of the plasma response close to termination is shown in Fig. 1. The evolution of profiles of electron temperature, density and pressure profiles from Thomson scattering $t=6.05$ s and $t = 6.10$ s indicate the plasma response due to two hydrogen pellets injected at $t=6.038$ s and 6.071s ($N=1.5 \times 10^{21}$ particles each). Timing and size of the pellets in the shot series (other shots not shown) has been varied and the shown case is an example of close to marginal sustainment of the plasma long (>800 ms) after pellet injection.

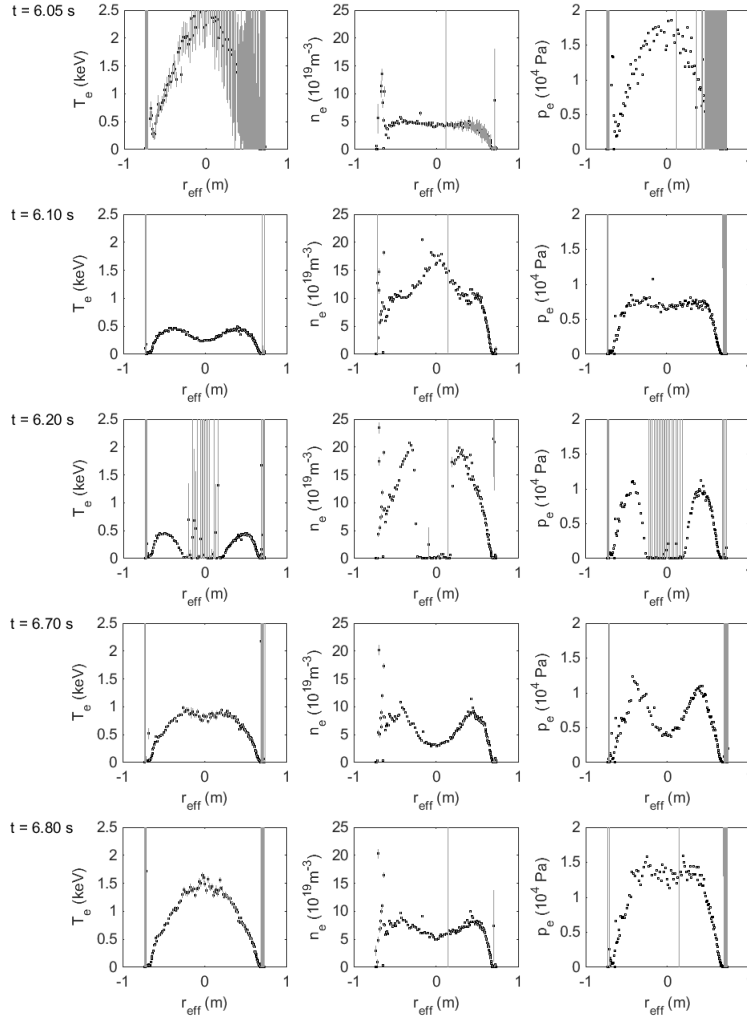


FIG. 1. Time evolution of electron temperature (left), density (middle) and pressure (right column) after pellet injection in LHD close to the operational density limit (from Thomson scattering). Pellets are injected at $t = 6.038, 6.0719$ s. The detection limit for T_e is around 5eV and multichannel interferometer measurements in similar discharges indicate a core density around $2 \times 10^{19} \text{m}^{-3}$ for the cold core region (refers to $t = 6.2$ s) [15].

The time-slice at $t = 6.20$ s shows a strong decrease of the electron pressure (with small measured temperatures and densities) to values below the detection limits of the Thomson scattering system. In the course of the discharge ($t = 6.70$ s), however, density profiles even leading to positive electron pressure gradients are observable in the detection range of the Thomson scattering. Therefore, even with the mentioned caveats, the measurements give clear evidence that a plasma almost terminated by fueling pellets can recover on confinement time scales (~ 100 ms). This conclusion is supported from the inspection of the visible light detected from a video camera. The characteristic structure of bright seams changes strongly in phases with small central electron temperature $T_e(0)$. The same phenomenology has been reported as a *temperature hole* [16].

3.2. TESPEL injection on LHD

An example for the plasma response due to a Gd impurity embedded in polystyrene pellets (TESPEL) is shown in FIG. 2. The comparison shows two cases of plasma response well after TESPEL injections in different discharges (cases are slightly different in terms of the encapsulated Gd impurity tracer). The specific ablation region for the discussed discharges has not been measured, but typically, the tracer ablation is around a normalized minor radius of about $\rho \sim 0.6$. Both discharges receive about almost the same amount of Gd atoms but are slightly different in terms of retained impurity atoms. This is reflected by the radiated power in the phase after TESPEL injection. Also after the phase of decay, the radiated power is higher than before TESPEL injection potentially indicating that a fraction of the impurities are retained. For the TESPEL injection in discharge #107489 ($(2.04 \pm 0.30) \times 10^{17}$ Gd atoms, red in FIG. 2), the radiated power appears to be slightly larger (also in stationary conditions are). The density appears to be visibly larger but is very similar for both cases. The central electron temperature

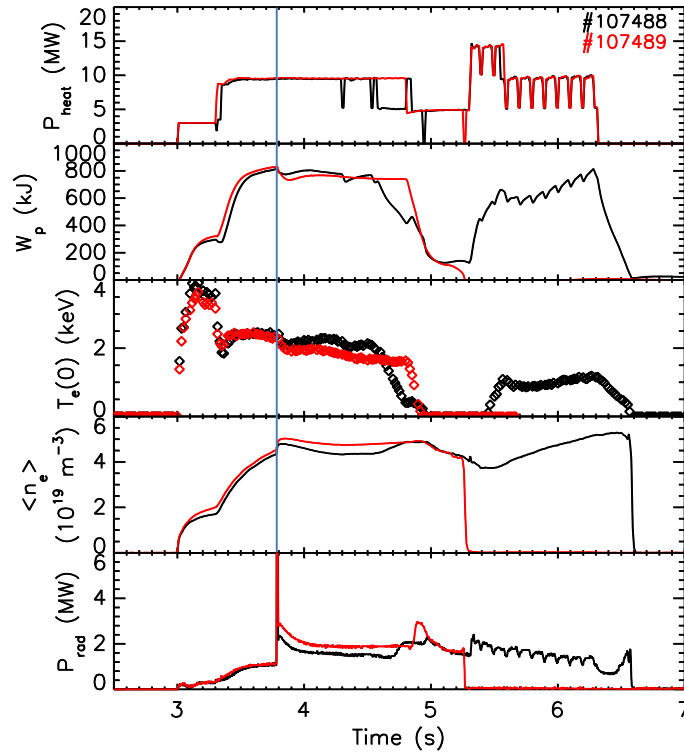


FIG. 2. Waveforms of heating power P_{heat} , plasma stored energy W_p , central electron temperature $T_e(0)$, mean density $\langle n_e \rangle$ and radiated power in response to Gd impurity pellets. Shot #107488 (black) receives a TESPEL with $1.98 \pm 0.30 \times 10^{17}$ particles, shot #107489 with $2.04 \pm 0.30 \times 10^{17}$ Gd atoms. The TESPEL is injected at $t = 3.8$ s (blue line).

is a little smaller than that in #107488 ($(1.98 \pm 0.30) \times 10^{17}$ Gd atoms, black waveforms in #107488). While the radiation power slowly decays after the plasma recovery for #107488, the emission intensity from Gd ions gradually decays according to the decay of the radiation power. This decay is accompanied by an increase of electron density and almost unchanged electron temperature. This implies that Gd atoms may be gradually exhausted from the confinement region.

Plasma response leading to termination or recovery is induced when the heating power is decreased. For #107488 (black), the heating power goes from 10 to 5 MW at ~ 4.6 s leading to a cooling of the plasma visible in the electron temperature. There is almost no response of the radiated power P_{rad} . Somewhat delayed, the radiated power increases after a dead-time of ~ 120 ms significantly leading to additional radiative cooling of the plasma (while the density stays virtually unaffected). The change of plasma energy dW_p/dt is about 1.5 MW in this period which is in the order of the radiated power. Shortly before the central temperature measurements gets to vanishing temperatures, a short recovery of the plasma heating is suspected to stabilize the electron temperature which is not measurable for about 500 ms. The temperature profiles (not shown here) resemble the temperature hole feature

[17] as reported for the fuelling pellet cases. $T_e(0)$ increases again after the heating power steps up but with a dead-time ~ 100 ms. During periods of temperature holes, $T_e(0) = 0$, the diamagnetic loop still measures plasma energies around 150 kJ indicating the hollow plasma pressure even with $T_e(0) = 0$. A full recovery of the plasma temperature is observed when the heating power is increased from 5 to about 14 MW and the temperature profiles appear as being filled up eventually leading to peaked temperature profiles.

For the second discharge #107489 (red in Fig. 2), the plasma also decays when the heating power is switched down. The loss of plasma energy is about $dW_p/dt \sim 3.3$ MW during the decay lasting around 150 ms. As for this case the plasma radiation increases to values up to ~ 3 MW. Both loss figures get much closer to the values of the heating power thus indicating that the discharge #107489 is much more affected by radiation and other losses than #107488. It is noted the increase of radiated power occurs when the central electron temperature falls below ~ 1 keV. Differently to #107488, the plasma energy is still not stabilizing in the period with vanishing central temperature ($T_e(0) = 0$) but is decaying further to show a collapse also in the plasma density within 50 ms at the end of the discharge. The specific time of the collapse coincides with a tripping of the plasma heating to vanishing heating power. Even a large increase of heating power after the short tripping does not lead to a recovery of the plasma as in shot #107488. It is concluded that the difference in retained Gd atoms from the TESPEL leads to the observed differences.

3.3. Plasma termination by LBO in Wendelstein 7-X

FIG. 3 shows an example of plasma termination on W7-X after massive tungsten injection by laser blow-off (with LBO pulses at 20 Hz starting at 23.64s (pulse separation 0.05s), some ten milligrams of tungsten in each LBO pulse). The energy decay is predominantly due to radiative cooling of the plasma. The electron temperature decays about a factor of two faster than a typical energy confinement time (~ 100 ms), while the plasma density remains almost constant (even slightly increasing). Since the density does not decrease, this observation provides evidence that energy losses are due to plasma radiation. Transport processes lead to cooling of the plasma and allowing a deeper penetration of the impurities released by LBO. For the power balance, however, transport induced losses appear to play a subordinate role. The plasma is finally terminated along with a strong increase of radiation and an increase of iron impurity lines (not shown). The overall mechanism could not be revealed and appears to be complicated. Possible reasons could be an overall cooling of the plasma and may indicate additional influx of impurities due to enhanced plasma wall interaction.

3.4. The specific spatio-temporal dynamics of the electron temperatures (measured by multi-channel electron-cyclotron emission radiometry (ECE) shown in Fig. 3) indicate local radiation effects. The innermost channel (ECE_12) indicates a longer cooling period. This is also supported from the bolometer detecting the core region of the plasma. The temperature dependence of the cooling rate (due to the abundance of ionization stages of impurities) could be mechanism leading to the different decay times in

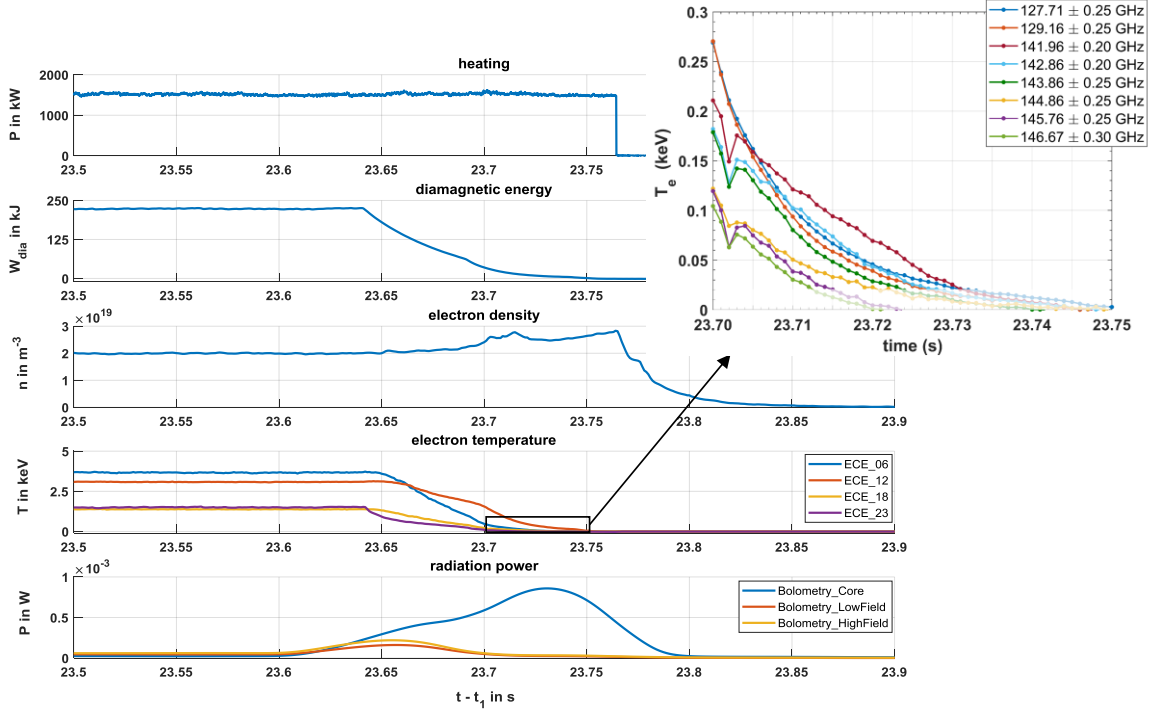


FIG. 3. Waveforms of heating power, diamagnetic energy, electron density, electron temperature, and radiated power (from different plasma regions) after massive tungsten laser blow-off at 23.640, 23.645 and 23.650 s. The inset shows the decay of radiation temperatures from different peripheral ECE channels on the low-field side (<140GHz) and the high-field side shortly before the plasma is cooled below the detection limits. Below 200 eV, the black-body assumption is not fulfilled and the data in the inset are covered accordingly.

the plasma region. Likewise, spatial dependencies are indicated in the LHD TESPEL case from the increasing radiation when the plasma cools down below an apparent recombination threshold. The inset of Fig. 3 shows peripheral ECE radiometer channels on the low field side (<140GHz) and high-field side. Below around 200eV, Rayleigh-Jeans law does not hold and the intensities do not reflect the temperature correctly. It is noted that a small transient cooling is detected for the high-field side shortly after 23.70s. Interestingly, video camera frames (not shown here) show shining, remnant traces of material at the same time. The different response on high- and low-field side channels indicate transient poloidal asymmetries

indicating the parallel heat conductivity becoming too low for fast equilibration on flux surfaces..
Plasma termination by fueling pellets and TESPEL and plasma recovery after TESPEL injection in TJ-II

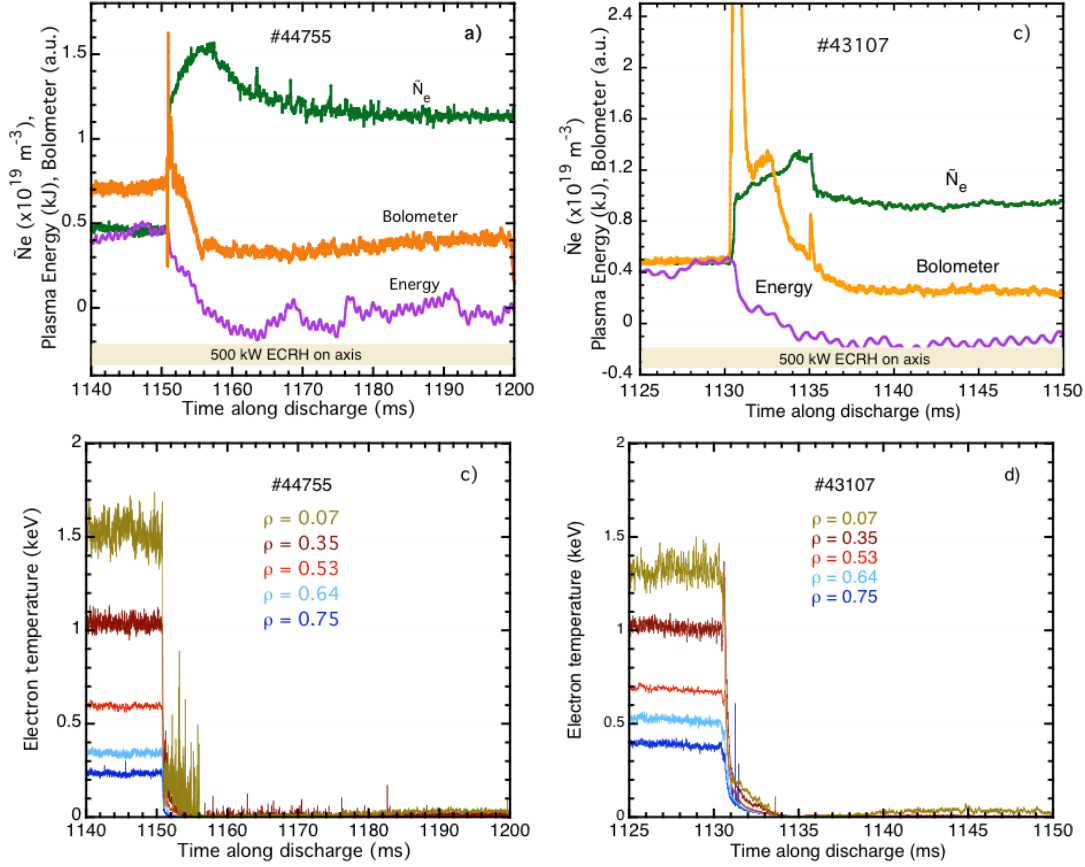


FIG. 4. Plasma termination by pellet injection in TJ-II: waveforms of line-averaged density, plasma energy and radiative power loss (top). Waveforms for selected minor radii from a multichannel ECE radiometer (bottom). (a) and (c) show the response for a hydrogen fuelling pellet entering the plasma at $t = 1150.57$ ms. (b) and (d) for a TESPEL entering the plasma at $t = 1130.7$ ms. For #44755, the pellet contains $\sim 1.87 \times 10^{17}$ H atoms. For #43107, the TESPEL contains 6.3×10^{17} atoms of H, an equal number of C atoms and 5×10^{16} S atoms. This is equivalent to $\sim 5 \times 10^{18}$ electron [17].

In TJ-II, the injection of a large cryogenic pellet ($> 1.5 \times 10^{19}$ H) into an on-axis ECRH discharge leads to rapid plasma termination. This is seen in Fig. 4 where the plasma experiences a collapse with rapid energy loss (< 10 ms) after pellet entry into the plasma. During this process radiation drops rapidly and a weak glow remains thereafter. Similarly, if a sufficiently large TESPEL (C_8H_8) is injected into the target discharge a comparable plasma termination occurs. For both TJ-II discharges considered here, #44755 and # 43107, the plasma particle content is almost 5×10^{18} particles while the ECRH cut-off density is $1.5 \times 10^{19} \text{ m}^{-3}$. Moreover, for hydrogen pellets injected into ECRH plasmas, the fuelling efficiency is typically $\sim 30\%$, so $\sim 5.6 \times 10^{18}$ particles are deposited in #44755 [18]. In contrast, for TESPEL pellets, 80% of its particles are deposited in the plasma core [K. J. McCarthy et al., EPL 120 (2017) 25001]. Thus, for both cases the ratios of pellet content to total post injection plasma content are $\geq 80\%$. For both situations, pellet injection induces an abrupt increase in plasma electron density from $5 \times 10^{18} \text{ m}^{-3}$ to $> 10^{19} \text{ m}^{-3}$ followed by a slower steady increase towards cut-off ($\bar{N}_e > 1.4 \times 10^{19} \text{ m}^{-3}$). In such cases no plasma recovery is observed, rather a cold dense plasma remains but is never reignited.

In contrast, in some instances, plasma recovery is found in TJ-II after a large TESPEL injection. Such a recovery is observed in Fig. 5, where a polystyrene pellet with sulphur tracer, $C_8H_8(S)$, is injected into an off-axis ECRH discharge (at $r/a = 0.34$). In this case, the initial post-injection rise in electron density is smaller than in Fig. 4, this being followed by a subsequent steady increase up to cut-off. This smaller abrupt density increase can be understood by considering that a large fraction of pellet electrons are carried by the carbon and sulphur atoms, resulting in a slow \bar{N}_e rise after pellet ablation as ionization continues during several milliseconds to C+6 and S+13[18]. This also results in a slower plasma energy decrease which falls to $\sim 50\%$ of the pre-injection value when the discharge reaches cut-off. From Thomson Scattering profiles taken before and after injection, it is seen that the plasma core does not cool completely (Fig. 5), rather a dense, but not cold, plasma column remains in its core. Finally, after several ten milliseconds of continued ECRH injection into the plasma, whose density remains high but below cut-off, it partially reignites with plasma energy increasing above pre-injection levels.

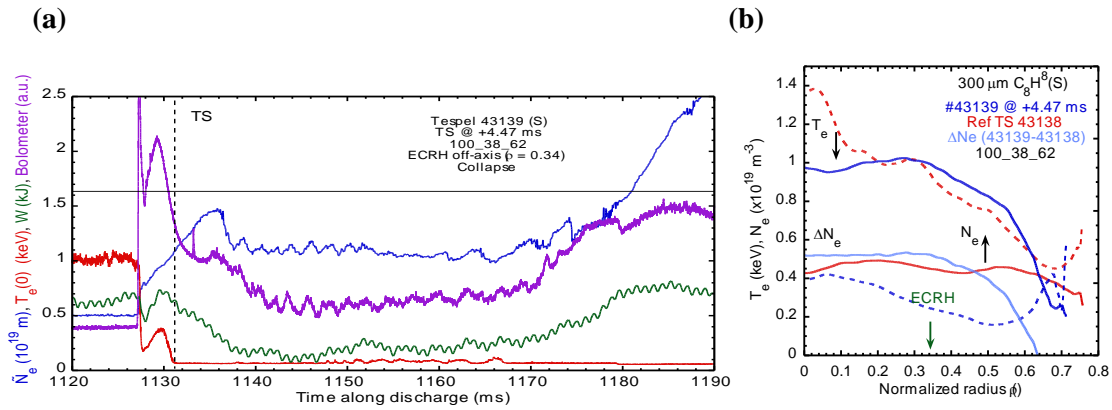


FIG. 4. (a) Waveforms of line-averaged electron density, central electron temperature, plasma energy and plasma radiation. (b) Electron density and temperature profiles from Thomson scattering during plasma decay compared to profiles from a reference discharge without TESPEL.

4. DISCUSSION AND SUMMARY

TABLE 1. CHARACTERIZATION OF PARTICLE INJECTION LEADING TO PLASMA TERMINATION

Device	Case	injected material	decay time
LHD	Excess fuelling	H_2	order of (100ms)
	TESPEL	Gd	~ 150 ms
W7-X	Excess LBO	W	~ 50 ms
TJ-II	Excess fuelling	H_2	< 5 ms
	TESPEL	C_8H_8	< 5 ms

The systematic comparison of plasma terminating events by cryogenic pellets, induced impurity injection or changes of the heating in stellarators and heliotrons gives evidence that the observed termination takes place on a time scale somewhat smaller than the energy confinement time. The cases investigated here are characterized by plasma cooling by large radiated power due to excess fuelling or impurity injection. A caveat is raised, however, due to differences for the cases documented here. This study serves as an initial paper about plasma terminating events and the study is considered to be neither comprehensive nor to document directly comparable cases; therefore the summarizing Table 1. serves as an initiation for a broader documentation.

Cases comparing TESPEL injection close to marginal termination with slightly higher core radiation indicate that the cooling rate in relation to the heating power ($P_{rad} \sim P_{heat}$) along with the number of radiating particles defines threshold conditions for the plasma collapse. Subsequent increase of the heating power was observed to lead to plasma recovery for the TESPEL injection. The specific reason for the short decay time observed on TJ-II remained unclear. The role of a lack of absorption due to density increasing towards cut-off complicates the analysis in general. The crucial role of plasma radiation is supported with the effect of tungsten radiation on W7-X collapses. Close to marginal termination, LHD shows very clearly the beneficial effect of confinement of the

vacuum field which gives rise to transient plasmas with cold regions in the center but may recover after typically 1s. It is to be investigated if temperature holes due to fueling pellet injection recover when the absorbed heating power is increasing during the recovery to go to lower $P_{\text{rad}}/P_{\text{heat}}$ ratios.

Typical time scales of plasma terminating events were found to be fractions of the energy confinement time and were related to radiated power from injected impurities (and thus the number of radiating particles). The observed time scales are some orders of magnitude larger than MHD time scales and appear to lead to relaxed requirements for plasma facing materials than required for fast terminating events. Recent observation of plasma termination in the course of changes of an intended change of the rational transform by electron cyclotron current drive [21], however, indicate that fast terminations can be intentionally induced by broadly applied current drive. These findings will be reported elsewhere. A comparison to tokamaks appears to be way too premature since it requires further disentanglement of underlying mechanisms. Ohmic heating, inducing non-linear coupling in resistivity and radiation is a player in tokamaks not showing up in helical devices.

In conclusion, the multi-machine comparison of plasma terminating events in this paper indicate that the vacuum confinement of stellarators and heliotrons differently to tokamaks has a benign impact in plasma terminating events due to excess material injection showing even the capability of helical currentless confinement devices for plasma recovery if exposed to not too high particle influx. In other points, this work is a clear demonstration that in helical devices with magnetic confinement ensured with the vacuum magnetic fields, the plasma recovery relies on the effective heating scheme in high density operational regime.. These findings appear to be relevant to the discussion of unintended exposure of material to a fusion plasma.

ACKNOWLEDGEMENTS

This work has been conducted under auspices of the IEA Technology Collaboration Programme on the Stellarator-Heliotron Concept.

This work has been carried out within the framework of the EUROfusion Consortium and has received funding from the Euratom research and training programme 2014-2018 and 2019-2020 under grant agreement No 633053. The views and opinions expressed herein do not necessarily reflect those of the European Commission. CS and NT acknowledge supports by the JSPS KAKENHI (Grant Nos. 23360415, 15H03759, and 15H04234), a fundamental budgetary support (Nos. ULHH012 and ULHH017), the Program for Enhancing Research Collaboration (UFEX105), the Young Researchers Supporting Program (UFEX106) of the National Institute for Fusion Science, the NIFS/NINS under Strategic International Research Exchange Promotion Program (UFEX402), and the NINS program of Promoting Research by Networking among Institutions (Grant No.01411702). KJM acknowledge support from MINECO (FIS2017-89326-F).

The authors are grateful to an anonymous referee for her/his comments.

REFERENCES

- [1] FUCHERT G., et al., Increasing the density in W7-X: benefits and limitation Preprint: 2018 IAEA Fusion Energy Conference, Gandhinagar [EX/3-5]
- [2] SUDO A., et al, Nucl. Fusion 30, 11 (1990).
- [3] ITOH, K. and ITOH, S.-I., J. Phys. Soc. Jpn. 57, 1269 (1988)
- [4] DINKLAGE A., et al., Nucl. Fusion **53** (2013) 063002.
- [5] KOMORI A., et al., Fusion Sci. Technol. **58** (2010) 1.
- [6] SAKAMOTO R., et al., Nucl. Fusion **52** (2012) 083006.
- [7] SUDO S., TAMURA N., Rev. Sci. Instrum. **83** (2012) 023503.
- [8] KLINGER T., et al., Plasma Phys. Contr. Fusion **59** (2017) 014018.
- [9] DIBON M., Entwicklung und Verbesserung eines Blower-Gun Pellet Injektors für die Anwendung in thermonuklearen Fusionsanlagen (in German), Master Thesis, Technical University Munich (2014).
- [10] WEGNER, Th., et al., Rev. Sci. Instrum. **89** (2018) 073505.
- [11] CASTEJON, F., et al., Nucl. Fusion **57** (2017) 102022.
- [12] MCCARTHY, K.J., et al., Nucl. Fusion **57** (2017) 056039.
- [13] TAMURA, N., et al., Rev. Sci. Instrum. **87** (2016) 11D619.

- [14] SAKAMOTO, R., et al., Rev. Sci. Instrum **84** (2013) 083504.
- [15] SUZUKI, C. et al, J. Phys. B: At. Mol. Opt. Phys. **45** (2012) 135002
- [16] MIYAZAWA, J., et al., Nucl. Fusion **48** (2008) 015003.
- [17] SUZUKI, C., et al., Plasma Phys. Control. Fusion **59** (2017) 014009.
- [18] McCARTHY, K.J., et al., Phys. Scripta **91**, 035061 (2018)
- [19] McCARTHY, K. J. et al., Nucl. Fusion **57** 056039 (2017)
- [20] McCARTHY, K. J., et al., Europhys. Lett. **120** (2017) 25001.
- [21] KLINGER, T., et al., Overview of first W7-X high-performance operation with island divertor, Preprint: 2018 IAEA Fusion Energy Conference, Gandhinagar [OV/4-1]